New anatomical information on the bohaiornithid *Longusunguis* and the presence of a plesiomorphic diapsid skull in Enantiornithes

Han Hu, Jingmai K. O'Connor, Min Wang, Stephen Wroe & Paul G. McDonald

To cite this article: Han Hu, Jingmai K. O'Connor, Min Wang, Stephen Wroe & Paul G. McDonald (2020): New anatomical information on the bohaiornithid *Longusunguis* and the presence of a plesiomorphic diapsid skull in Enantiornithes, Journal of Systematic Palaeontology, DOI: 10.1080/14772019.2020.1748133

To link to this article: https://doi.org/10.1080/14772019.2020.1748133

View supplementary material 🗗

Published online: 20 Apr 2020.

Submit your article to this journal 🗗

View related articles 🗗

View Crossmark data 🗗

Full Terms & Conditions of access and use can be found at
https://www.tandfonline.com/action/journalInformation?journalCode=tjsp20

Taylor & Francis
Taylor & Francis Group

Check for updates

New anatomical information on the bohaiornithid *Longusunguis* and the presence of a plesiomorphic diapsid skull in Enantiornithes

Han Hu[a]* iD, Jingmai K. O'Connor[b,c], Min Wang[b,c] iD, Stephen Wroe[a] and Paul G. McDonald[a] iD

[a]*Zoology Division, School of Environmental and Rural Sciences, University of New England, Armidale, NSW 2351, Australia;* [b]*Key Laboratory of Vertebrate Evolution and Human Origins, Institute of Vertebrate Paleontology and Paleoanthropology, Chinese Academy of Sciences, 10010 Beijing, PR China;* [c]*Chinese Academy of Sciences Center for Excellence in Life and Paleoenvironment, 10010 Beijing, PR China*

Bohaiornithidae is currently the most diverse recognized family of Early Cretaceous enantiornithines, with unique morphology of the rostrum and pedal digits. Here we describe a second specimen of the bohaiornithid *Longusunguis kurochkini* from the Jiufotang Formation. This specimen provides new anatomical information regarding this taxon, in particular clarifying uncertain aspects of enantiornithine cranial morphology. The rarely preserved postorbital is completely preserved on both sides of the skull, confirming the presence of a complete postorbital bar in some enantiornithines. This suggests that the plesiomorphic diapsid skull was retained by at least some basal enantiornithines and the infratemporal fenestra in Ornithothoraces may have been lost independently multiple times, providing a better understanding of cranial evolution from non-avian dinosaurs to modern birds.

Keywords: Bohaiornithidae; postorbital; cranial evolution; Early Cretaceous

Introduction

Since the 1990s, thousands of exceptionally preserved stem bird (non-neornithine Aves) fossils have been uncovered from the Lower Cretaceous Jehol Biota of north-eastern China. Persisting for over 10 million years from 130.7–120 Ma (Swisher *et al*. 2002; He *et al*. 2004, 2006), the Jehol avifauna is the most diverse Mesozoic avifauna currently known to science, preserving numerous stem avian lineages found nowhere else in the world (Zhou 2014). These spectacular discoveries are dominated in terms of both taxonomic diversity and numbers of specimens by Enantiornithes (Aves: Ornithothoraces), the dominant clade of land birds throughout the Cretaceous (O'Connor 2009; M. Wang & Zhou 2017a). Bohaiornithidae is the most diverse enantiornithine clade known, with six genera: *Bohaiornis*, *Gretcheniao*, *Longusunguis*, *Parabohaiornis*, *Shenqiornis*, *Sulcavis* and *Zhouornis* (X. Wang *et al*. 2010; D. Hu *et al*. 2011; O'Connor *et al*. 2013; Z. Zhang *et al*. 2013; Li *et al*. 2014; M. Wang *et al*. 2014; Y. Zhang *et al*. 2014; Chiappe *et al*. 2019), all known from the Jehol Biota with most from the Jiufotang Formation (125–120 Ma, He *et al*. 2004; M. Wang *et al*. 2014). The phylogenetic position of this clade within Enantiornithes is unstable, but its

monophyly has been supported in several phylogenetic studies (M. Wang *et al*. 2014, 2016; H. Hu & O'Connor 2017; M. Wang & Zhou 2019), with slight variations in some analyses, for example the inclusion of *Fortunguavis* in H. Hu & O'Connor (2017). This group is characterized by the shared presence of a relatively robust rostrum, subconical teeth that are relatively more robust than those of other enantiornithines, bluntly expanded omal ends of the furcula, and an elongate ungual on pedal digit III (M. Wang *et al*. 2014). These unique features, together with the fairly large body size and robust morphology of all known members, suggest that this clade was ecologically specialized relative to other Jehol enantiornithines (M. Wang *et al*. 2014; Y. Zhang *et al*. 2014): the enamel grooves in *Sulcavis*, together with the robust rostrum and dentition, might represent adaptations for hard diet items (O'Connor *et al*. 2013; O'Connor 2019), while preliminary analysis of pedal proportions and claw curvature has been interpreted as similar to that of extant arboreal birds (M. Wang *et al*. 2014).

Here we report a new specimen referable to *Longusunguis kurochkini* (IVPP V18693). This taxon was previously known only from the holotype specimen, IVPP V17964, which preserves rare cranial features, such as the presence of a maxillary foramen and

---

*Corresponding author. Email: huhan@ivpp.ac.cn

elements that have been tentatively identified as ptery-goids. The referred specimen (IVPP V18693) is nearly complete and articulated, revealing new morphological details pertaining to the pectoral and pelvic girdles, foot and the cranium, complementing data from the holotype. Most remarkably, IVPP V18693 clearly preserves both postorbitals, elements which are rarely present in Mesozoic ornithothoracine specimens. The postorbital is unreduced and separates the infratemporal and the supratemporal fenestrae in non-avian dinosaurs, contributing to an akinetic diapsid skull. In contrast, this element is strongly reduced to a process fused to the frontal in modern birds. Thus, the morphological modification and reduction of the postorbital are critical to understand a key transition during the early evolution of birds: the appearance of a kinetic skull from the akinetic condition of non-avian dinosaurs, which has consistently attracted the attention of the researchers (Zusi 1984; Hou *et al*. 1999; Holliday & Witmer 2008; Bhullar *et al*. 2016).

Material and methods

Anatomical terminology follows Baumel & Witmer (1993), using the English equivalents of the Latin nomenclature. Computed laminography (CL) scanning of the skull and the whole slab of IVPP V18693 was generated using the X-ray microcomputed laminography scanner at the Key Laboratory of Vertebrate Evolution and Human Origin of CAS, IVPP, Beijing, China.

In order to test the taxonomic hypothesis that IVPP V18693 is referable to *Longusunguis kurochkini*, this specimen was added into a modified version of the M. Wang & Zhou (2019) dataset for phylogenetic analysis using TNT v. 1.5 (Goloboff & Catalano 2016). See Supplementary materials S1 and S2 for the character list and dataset. We ran a heuristic search conducting 1000 replications of tree bisection reconnection (TBR) branch swapping and saving 10 trees per replication, which returned 270 most parsimonious trees (MPTs) of length 1258 steps. A second round of TBR branch swapping returned 504 MPTs of 1257 steps.

Institutional abbreviations

BMNHC: Beijing Natural History Museum, Beijing, China; **CNU**: Capital Normal University, Beijing, China; **DNHM**: Dalian Natural History Museum, Dalian, Liaoning, China; **IVPP**: Institute of Vertebrate Paleontology and Paleoanthropology, Chinese Academy of Sciences, Beijing, China; **LPM**: Liaoning Paleontology Museum, Shenyang, Liaoning, China;

NIGP: Nanjing Institute of Geology and Paleontology, Chinese Academy of Sciences, Nanjing, China.

Systematic palaeontology

Aves Linnaeus, 1758
Ornithothoraces Chiappe, 1995
Enantiornithes Walker, 1981
Bohaiornithidae M. Wang *et al*., 2014
Genus ***Longusunguis*** M. Wang *et al*., 2014
Longusunguis kurochkini M. Wang *et al*., 2014
(Figs 1–4)

Holotype. IVPP V17964, a nearly complete and articulated subadult skeleton dorsally exposed in a single slab (M. Wang *et al*. 2014).

Referred material. IVPP V18693, a nearly complete and articulated subadult skeleton primarily exposed in dorsal view in a single slab; the feathers are poorly preserved.

Occurrence. Lingyuan, Liaoning, China; Jiufotang Formation (Lower Cretaceous).

Emended diagnosis. *Longusunguis kurochkini* can be distinguished from other bohaiornithids by the following combination of features: maxilla bearing four teeth (new feature) and an accessory fenestra on the jugal process; nasal with a centrally located round fenestra (new feature); lacrimal with elongate excavation on the caudal margin of the ventral ramus; postorbital bearing long, delicate and tapered jugal process, and short frontal and squamosal processes (new feature); squamosal triradiate with postorbital process unforked (new feature); lateral margin of coracoid more convex than in other bohaiornithids; acromion process strongly projecting dorsally; and pygostyle equal to or longer than the tarsometatarsus (modified from M. Wang *et al*. 2014).

Ontogenetic status. The premaxillae corpora and rostral base of the frontal processes are fused in IVPP V18693, suggesting that this individual was nearing skeletal maturity. The synsacrum and pygostyle are completely fused and the proximal tarsals are fused to the distal end of tibia forming a true tibiotarsus, confirming that the specimen is not a juvenile or young subadult. However, the distal ends of the lateral trabeculae and the xiphoid process of the sternum, the sternal margin of the coracoid and the epiphyses of some limb bones (e.g. femur and tibiotarsus) are coarse and slightly porous, indicating incomplete ossification and precluding IVPP V18693 from recognition as a fully mature individual. Furthermore, the semilunate carpal is not fused to the metacarpals and the distal tarsals are not fused to

the proximal metatarsals. Together, this information suggests that IVPP V18693 was a subadult nearing maturity at the time of death.

Description

The following anatomical description is based on IVPP V18693 (Fig. 1; Table 1), focusing on morphologies not preserved in the holotype (IVPP V17964) with comparisons to other known bohaiornithids.

Skull

The skull of IVPP V18693 is preserved in dorsal view with most elements preserved *in situ*. The mandibles are largely overlapped by the skull with only the distal portions exposed (Fig. 2).

The premaxillae are nearly complete with the slender frontal process much longer than the maxillary process. The premaxillae corpora and the rostral third of the frontal processes are medially fused; the caudal portion of the frontal processes remain separated (Fig. 3A). Similar partial fusion of the premaxillae can also be
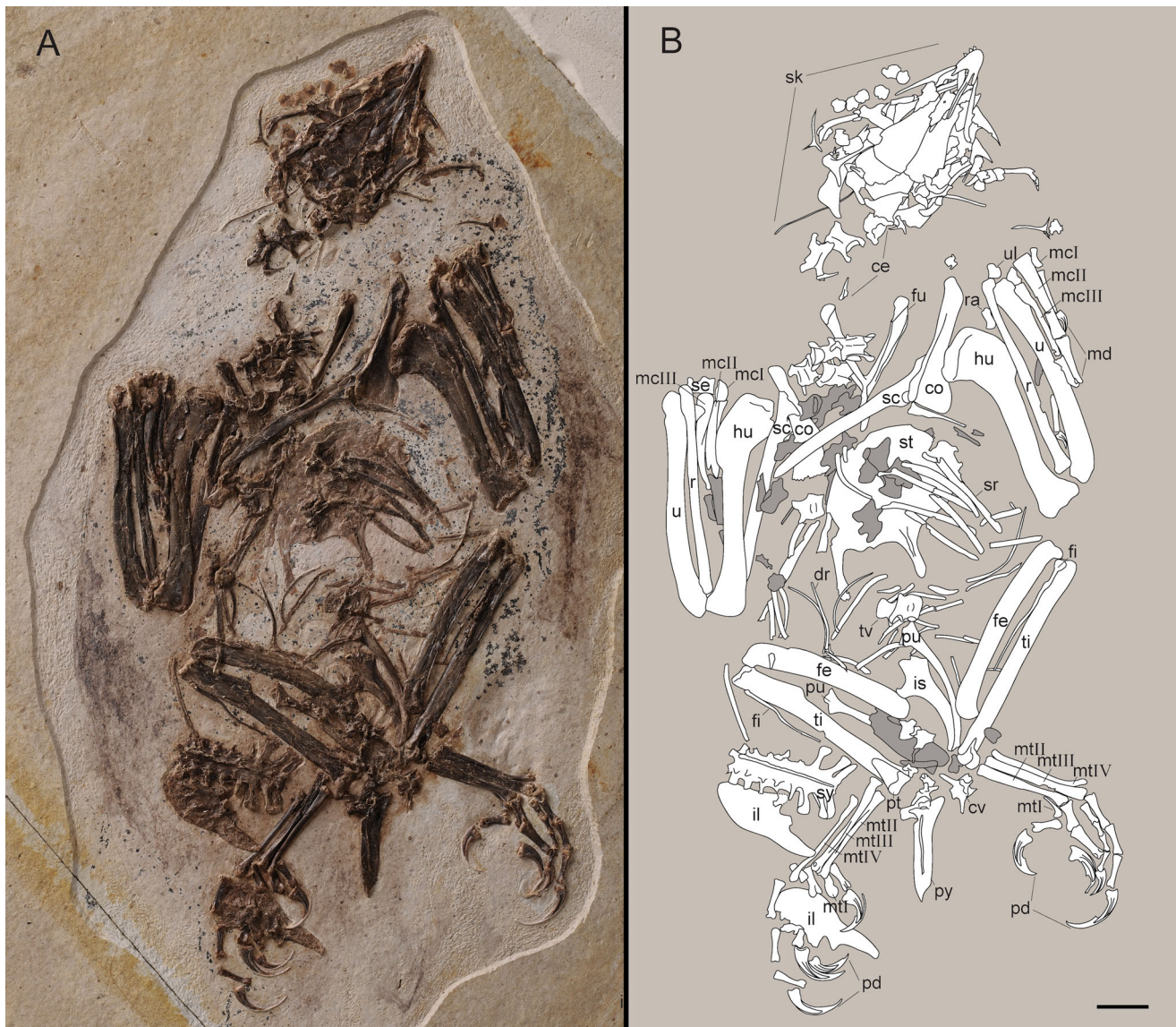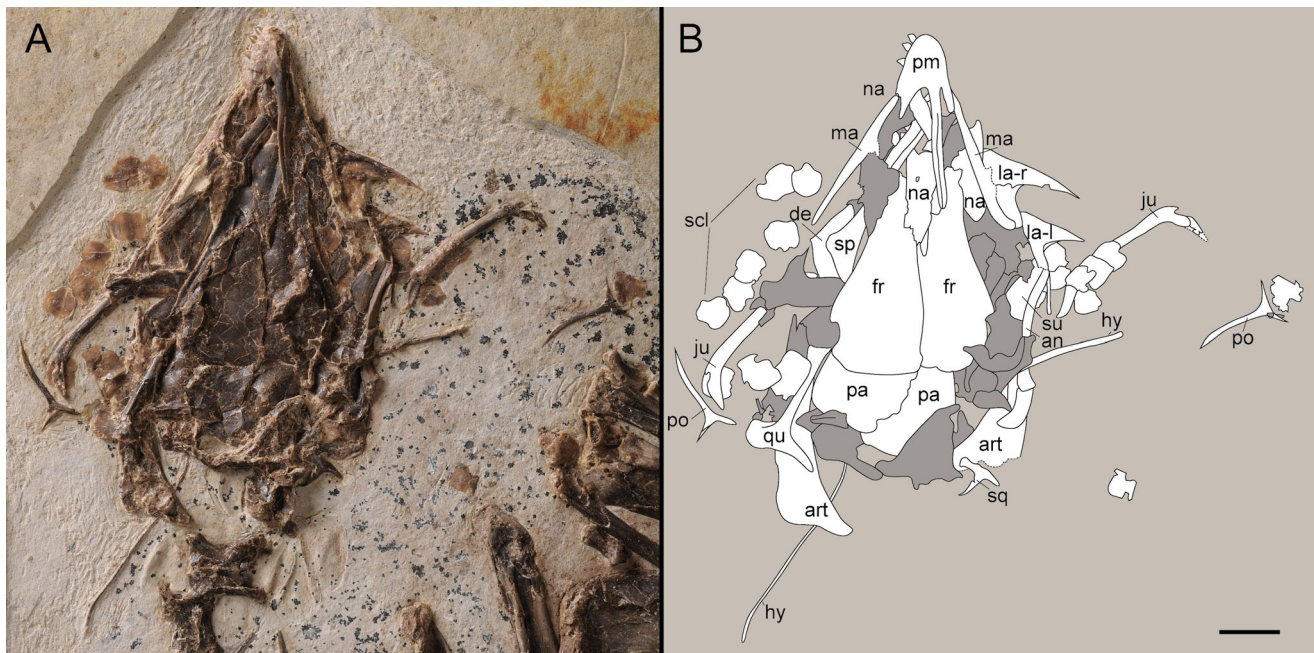

Figure 1. A, photograph and **B,** camera lucida drawing of *L. kurochkini* (IVPP V18693), with crushed parts in grey and margins indicated from the imprints in dashed lines. **Abbreviations: ce**, cervical vertebrae; **co**, coracoid; **cv**, caudal vertebrae; **dr**, dorsal rib; **fe**, femur; **fi**, fibula; **fu**, furcula; **hu**, humerus; **il**, ilium; **is**, ischium; **mcI–III**, metacarpals I–III; **md**, manual digits; **mtI–IV**, metatarsals I–IV; **pd**, pedal digits; **pt**, proximal tarsals; **pu**, pubis; **py**, pygostyle; **r**, radius; **ra**, radiale; **sc**, scapula; **se**, semilunate carpal; **sk**. skull; **sr**, sternal rib; **st**, sternum; **sy**, synsacrum; **ti**, tibiotarsus; **tv**, thoracic vertebrae; **u**, ulna; **ul**, ulnare. Scale bar = 1 cm.

Table 1. Measurements (in mm) of *Longusunguis* (IVPP V18693). **Abbreviations: l**, left; **r**, right. * indicates preserved length.

Element	Measurement	Element	Measurement
Synsacrum length	21.2	Metatarsal I length (r)	5.2
Pygostyle length	19.4	Metatarsal II length (r)	18.6
Clavicular rami length	18	Metatarsal III length (r)	20.5
Coracoid height (r)	25.6	Metatarsal IV length (r)	19.3
Scapula length (r)	37.1*	Pedal phalanx I-1 length (r)	5.8
Humerus length (r)	38.6	Pedal phalanx I-2 length (r)	9.2
Ulna length (r)	42.2	Pedal phalanx II-1 length (r)	4.8
Radius length (r)	39.3	Pedal phalanx II-2 length (r)	7.6
Alular metacarpal length (r)	3.9	Pedal phalanx II-3 length (r)	10.1
Major metacarpal length (r)	17.2	Pedal phalanx III-1 length (r)	7.2
Minor metacarpal length (l)	18.6	Pedal phalanx III-2 length (r)	5.8
Alular phalanx-1 length (r)	8.5	Pedal phalanx III-3 length (r)	6.5
Alular phalanx-2 length (r)	4.7*	Pedal phalanx III-4 length (r)	11.9
Major phalanx–1 length (r)	9.8	Pedal phalanx IV-1 length (r)	3.9
Ilium length (r)	23.2	Pedal phalanx IV-2 length (r)	3.3
Femur length (r)	37.8	Pedal phalanx IV-3 length (r)	3.1
Tibiotarsus length (r)	44.6	Pedal phalanx IV-4 length (r)	4.2
Fibula length (r)	25.5*	Pedal phalanx IV-5 length (r)	7.4

Figure 2. **A,** photograph and **B,** camera lucida drawing of the skull of *L. kurochkini* (IVPP V18693), with crushed parts in grey and margins indicated from the imprints in dashed lines. **Abbreviations: an**, angular; **art**, articular; **de**, dentary; **fr**, frontal; **hy**, hyoid; **ju**, jugal; **l**, left; **la**, lacrimal; **ma**, maxilla; **na**, nasal; **pa**, parietal; **pm**, premaxilla; **po**, postorbital; **qu**, quadrate; **r**, right; **scl**, scleral ossicles; **sp**, splenial; **sq**, squamosal; **su**, surangular. Scale bar = 5 mm.

observed in two other bohaiornithid specimens: the holotype of *L. kurochkini* (IVPP V17964: M. Wang *et al.* 2014) and a referred specimen of *Bohaiornis guoi* (IVPP V17963: Li *et al.* 2014), suggesting that partial fusion of the premaxillae is a shared feature of bohaiornithids. Rostrally fused premaxillae with separated frontal processes have also been previously reported in several enantiornithines, including the Early Cretaceous

Linyiornis and *Eoenantiornis*, and the Late Cretaceous *Gobipteryx* (O'Connor & Chiappe 2011; Y. Wang *et al.* 2016), while complete fusion is only documented in *Shangyang graciles* (M. Wang & Zhou 2019). Typical of other enantiornithines, four premaxillary teeth are revealed in the CL scans with the caudal-most tooth buried in the matrix (O'Connor & Chiappe 2011). *Bohaiornis* (LPM B00167) and IVPP V17963 also have

four premaxillary teeth (D. Hu *et al.* 2011), whereas *Zhouornis* (CNUVB-0903) and *Parabohaiornis* (IVPP V18691) apparently preserve only three premaxillary teeth, which led to the previous suggestion that this clade may be characterized by the presence of only three premaxillary teeth (Z. Zhang *et al.* 2013; O'Connor 2019). At this time, we cannot determine whether the absence of the fourth premaxillary tooth in these latter two taxa is an artefact of preservation or due to interspecific variation. As in the holotype, the shape of the premaxillary teeth in IVPP V18693 are typical of bohaiornithids, with sharply tapered and caudally recurved tips, convex labial and flat lingual surfaces (O'Connor *et al.* 2013; Z. Zhang *et al.* 2013; Li *et al.* 2014; M. Wang *et al.* 2014; Y. Zhang *et al.* 2014). Enamel ornamentation on the lingual surface is confirmed absent in this taxon.

Both maxillae are preserved in articulation with the premaxillae. The ascending process and adjacent region is crushed, preventing identification of the maxillary fenestra that perforates the base of the jugal process of the maxilla in other bohaiornithids, including the holotypes of *L. kurochkini*, *Bohaiornis guoi* (LPM B00167) and *Zhouornis hani* (CNUVB-0903) (D. Hu *et al.* 2011; Z. Zhang *et al.* 2013; M. Wang *et al.* 2014). The maxillary dentition of bohaiornithids was previously poorly known, with only *Zhouornis* (BMNHC Ph 756) described as having three maxillary teeth (Y. Zhang *et al.* 2014). CL data clearly reveals four alveoli in the rostral portion of the maxilla (Fig. 3H). Based on alveolar morphology, we infer that the maxillary teeth were similar in size to the premaxillary teeth. The rostral two teeth nearly contact each other, whereas the caudal two are separated by a diastema that is nearly as long as the mesiodistal length of the teeth themselves.

The broad plate-like bone slightly overlapped by the frontal processes of the premaxillae is identified as the left nasal. The nasal is perforated by a small rounded fenestra (Fig. 3A), which has previously only been observed in *Pengornis houi* among stem birds (Zhou *et al.* 2008; O'Connor & Chiappe 2011). The fenestra is centrally located and closer to the lateral margin, similar to the condition in *Pengornis*. The right nasal is covered by the maxilla and frontal with only the caudal margin exposed, which is bluntly tapered defining an angle of approximately 80°.

Both lacrimals are exposed in lateral view. The left lacrimal is nearly complete; however, the distal portion of the ventral (descending) ramus is overlapped by other elements. Visible in the CL image, the slender distal portion of the ventral ramus of the lacrimal is preserved underneath the right surangular (Fig. 3F). The lacrimal is 'T'-shaped similar to that of *Parabohaiornis* and
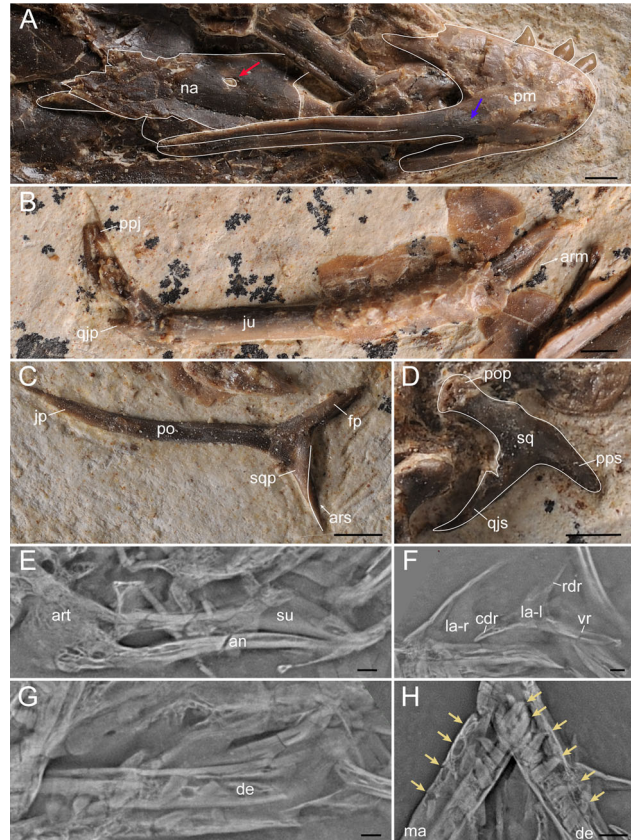

Figure 3. Detailed photographs of **A,** partial rostrum; **B,** right jugal; **C,** left postorbital; and **D,** right squamosal; and CL images showing **E,** right postdentary mandible; **F,** lacrimals; **G,** left dentary; and **H,** maxillary and dentary teeth of *L. kurochkini* (IVPP V18693). Arrows indicate the fenestra in the nasal (A, in red to the left), the fused corpus of the premaxilla (A, in blue to the right), the locations of the maxillary and dentary teeth (H, in yellow) and white lines indicate articular surfaces. **Abbreviations: an**, angular; **arm**, articular surface for maxilla on jugal; **ars**, articular surface for squamosal in postorbital; **art**, articular; **cdr**, caudodorsal ramus; **de**, dentary; **fp**, frontal process of postorbital; **jp**, jugal process of postorbital; **ju**, jugal; **l**, left; **la**, lacrimal; **ma**, maxilla; **na**, nasal; **pm**, premaxilla; **po**, postorbital; **ppj**, postorbital process of jugal; **pps**, postorbital process of squamosal; **pop**, postcotyloid process of squamosal; **qjp**, quadratojugal process of jugal, **qjs**, quadratojugal process of squamosal; **r**, right; **rdr**, rostrodorsal ramus; **sq**, squamosal; **sqp**, squamosal process of postorbital; **su**, surangular; **vr**, ventral ramus. Scale bar = 1 mm.

most other enantiornithines (M. Wang *et al.* 2014). The ventral ramus is longer than the rostrodorsal and caudodorsal rami and demarcates the caudal margin of the antorbital fenestra cranioventrally. The ventral ramus is excavated as in *Parabohaiornis* and *Pengornis* (O'Connor & Chiappe 2011; M. Wang *et al.* 2014). The dorsal margin is straight, whereas it is concave in *Pengornis* (Zhou *et al.* 2008).

Both jugals are preserved disarticulated; the right is partially overlapped by scleral ossicles (Fig. 3B) and the left is overlapped rostrally by an unidentified element. The tapered rostral end of the maxillary process is deflected dorsally, suggesting a dorsal-ventral contact with the maxilla along the ventral margin, as in the *L. kurochkini* holotype, *Bohaiornis* and *Pterygornis* (D. Hu *et al*. 2011; M. Wang *et al*. 2014, 2016). The caudal end of the jugal is forked forming a small caudally directed process and a longer and larger dorsocaudally directed process. Based on their orientation, we identify the shorter ramus as the quadratojugal process and the longer ramus as the postorbital process.

A small triradiate element preserved in the caudal right corner of the skull is identified as the squamosal (Fig. 3D). The three processes are similar in length. The sharply pointed process is most likely the ventrally oriented quadratojugal (descending) process; the dorsal process with the slightly expanded distal margin is identified as the caudal postcotyloid process; and the other gradually tapered dorsal process is identified as the postorbital process. The squamosal is only otherwise known in *Archaeopteryx* (Elzanowski & Wellnhofer 1996) and the juvenile enantiornithine LP 4450 (Sanz *et al*. 1997), and in both of these taxa it is also triradiate. However, we cannot conclusively exclude the possibility that there is another process for this specimen buried in the matrix.

Two triradiate elements preserved near the jugals are identified as the disarticulated postorbitals (Figs 2A, B, 3C). One process is extremely elongated and tapered distally and is identified as the jugal process of the postorbital. The short and dorsally deflected process is identified as the frontal process. The sharply tapered squamosal process is nearly as long as the frontal process and has a slightly concave dorsal surface, which is inferred to be the articular surface for the squamosal. The jugal process is approximately 2.7 times longer than the squamosal process. Compared to the broad triangular-shaped postorbital in *Sapeornis*, the postorbital of *Longusunguis* is much more delicate and the jugal process is proportionately longer, somewhat resembling the condition in the enantiornithine LP4450 and *Archaeopteryx* (Sanz *et al*. 1997; Rauhut *et al*. 2018).

The unfused frontals are tapered rostrally and expanded caudally as in other Mesozoic birds. They are approximately twice as long as the parietals, which is typical of ornithothoracines (O'Connor & Chiappe 2011). The morphology of the left quadrate is similar to that in other bohaiornithids, such as *Zhouornis* (Z. Zhang *et al*. 2013) and the fragment preserved in the holotype of *L. kurochkini*. The otic process is dorsoventrally elongated and oriented perpendicular to the

mandibular condyles. The dorsal margin of the otic process appears flat to weakly concave and is angled dorsolateral-ventromedially. The lateral mandibular condyle is larger than the medial condyle, as in the holotype.

At least 17 thin plate-like sclerotic ossicles are preserved disarticulated around the skull; eight or more are preserved on the right side and nine on the left. These square-shaped ossicles have rounded margins.

The mandibles are largely covered by the cranium in IVPP V18693 but are well preserved in the holotype. In the former, the left dentary and splenial are partially exposed through the naris and the antorbital fenestra. The dentary is straight and unforked caudally with a ventrally declined caudal margin (Fig. 3G), as observed in the holotype and typical of ornithothoracines (O'Connor & Chiappe 2011). Although overlapped by other elements, CL scans indicate that a total of six teeth are present in the right dentary (Fig. 3H); thus, the complete dentition of *Longusunguis* consists of four premaxillary teeth, four maxillary teeth and six dentary teeth. The dentary teeth are morphologically similar to those of the holotype, being sharply tapered with caudally recurved apices. The new specimen is consistent with the holotype in the relative positions of the dentary teeth: the first two are adjacent; the middle two are separated by a diastema measuring half of the mesiodistal length of the teeth themselves and the diastema separating the caudal two teeth is roughly equal in length to the mesiodistal lengths of the teeth themselves. The right surangular and angular are overlapped by other bones and are identified in the CL scan (Fig. 3E). The cranial portion of the surangular is dorsoventrally expanded. The angular is rod-like.

Vertebral column and ribs

The vertebral series is disarticulated and poorly preserved. At least nine cervical vertebrae are preserved, which are slightly craniocaudally elongate. A weakly developed ventral keel is visible on a cranial cervical vertebra preserved partially overlapping the furcula (Fig. 4C). At least seven thoracic vertebrae are preserved, which are disarticulated over and around the sternum. The most complete vertebra is preserved caudal to the sternum; the length and width of the vertebral body are nearly equal and the lateral surface is deeply excavated, as is typical of enantiornithines (Chiappe & Walker 2002). Neural spines are well developed and caudally displaced over the centra.

In IVPP V18693 the synsacrum is complete but has been displaced with the left ilium to lie below the left tibiotarsus; this element is broken into five pieces in the holotype. The sacrals are completely fused with no remaining sutures visible between intervening vertebrae
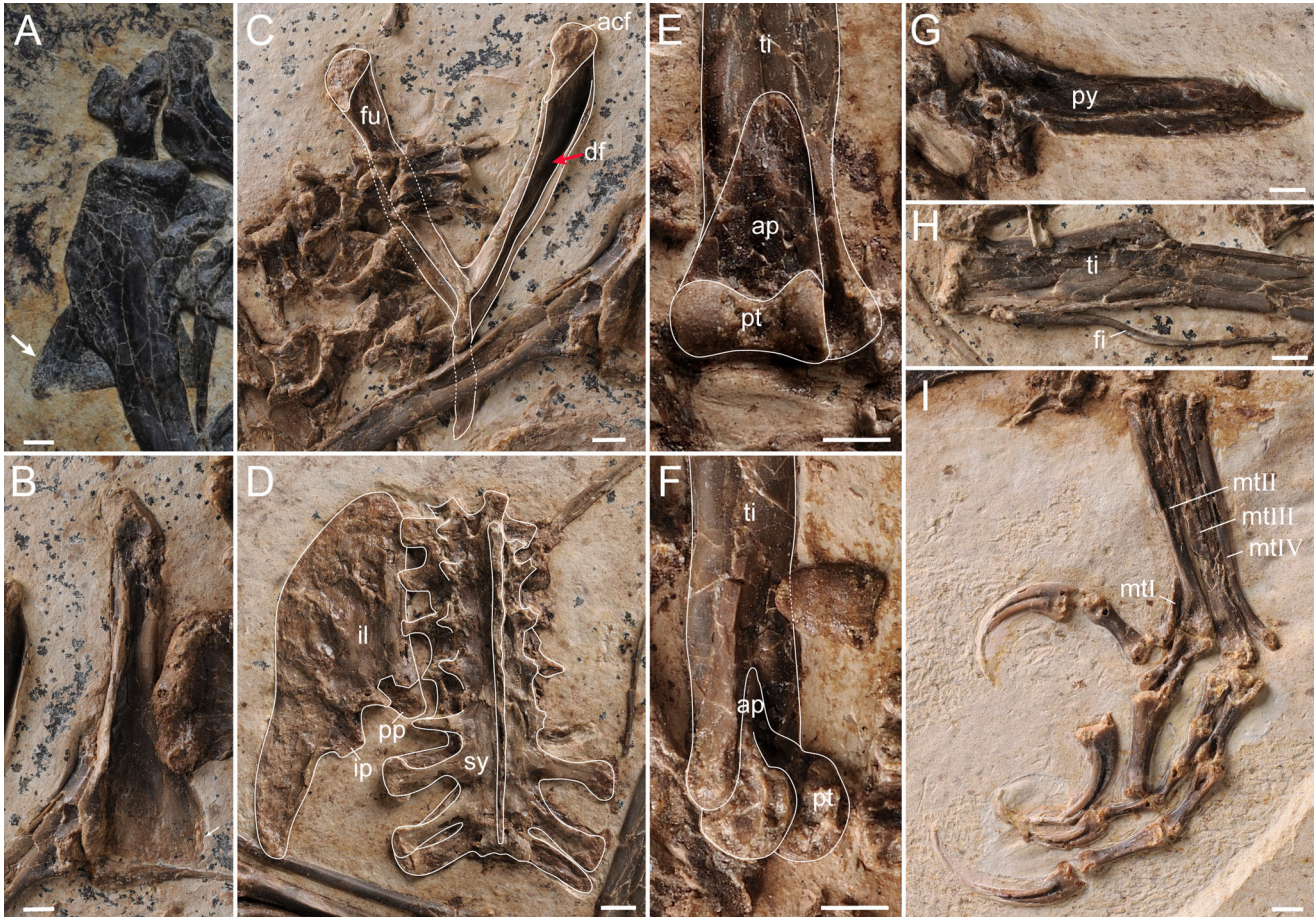
Figure 4. Detailed photographs of *L. kurochkini* (IVPP V18693). **A,** left coracoid; **B,** right coracoid; **C,** furcula; **D,** synsacrum and ilium; **E,** left distal tibiotarsus; **F,** right distal tibiotarsus; **G,** pygostyle; **H,** left tibiotarsus and fibula; and **I,** right foot. Dashed lines indicating the putative overlapping parts. White arrow (A) indicates the convex lateral margin of the coracoid and the red arrow (C) indicates the deeply excavated area in the dorsal surface of the furcula. **Abbreviations: acf**, articular surface for coracoid on furcula; **ap**, ascending process; **df**, dorsal furrow; **fi**, fibula; **fu**, furcula; **il**, ilium; **ip**, ischiac pedicle of ilium; **mtI–IV**, metatarsals I–IV; **pp**, pubic pedicle of the ilium; **pt**, proximal tarsals; **py**, pygostyle; **sy**, synsacrum; **ti**, tibiotarsus. Scale bar = 2 mm.

(Fig. 4D). Eight vertebrae are identified based on their transverse processes, which is consistent with the number in the holotype (seven or eight estimated) and with that number in other bohaiornithids, as is typical of enantiornithines (M. Wang *et al.* 2014). The fused neural spines of the sacral vertebrae form a spinous crest that extends for the entire length of the dorsal surface. The transverse processes of the cranial five sacral vertebrae are straight and short, and less than half the width of their vertebral bodies. The caudal three transverse processes are much longer, approaching the width of their centra, and are more robust with slightly expanded lateral extremities. The transverse processes of the cranial six vertebrae are laterally oriented, whereas the caudal-most two transverse processes are caudolaterally oriented and appear to contact each other at the lateral extremities.

Five free caudal vertebrae are preserved disarticulated cranial to the pygostyle. The best-preserved caudal is located near the right foot. It has caudolaterally directed transverse processes, which are nearly equal in length to the centrum width. The craniocaudally elongated pygostyle is preserved in lateral view and is nearly equal in length to metatarsal III, whereas it is slightly longer than metatarsal III in the holotype (Fig. 4G; Table 1; M. Wang *et al.* 2014). The caudal end is gradually tapered as in bohaiornithids (M. Wang *et al.* 2014), rather than abruptly constricted as in other enantiornithines (Chiappe & Walker 2002; H. Hu *et al.* 2015). A weakly developed crest is present on the lateral surface, which could be the remnants of a ventrolateral process similar to that in *Zhouornis* (BMNHC Ph756: Y. Zhang *et al.* 2014). Typical of enantiornithines, the pygostyle is tetraradiate in proximal view (Chiappe *et al.* 2002). The

short and craniodorsally directed dorsal processes end level with the cranial margin of the pygostyle body, whereas the ventral processes extend beyond the cranial margin.

Six rod-like elements preserved adjacent to the right of the sternum are tentatively identified as sternal ribs, based on their relatively straight and robust morphology compared to the curved and slender dorsal ribs in other known enantiornithines (M. Wang *et al*. 2016; M. Wang and Zhou 2017b). However, if correctly identified these sternal ribs are proportionately longer than in most other enantiornithines (F. Zhang *et al*. 2001; O'Connor *et al*. 2009, 2011), so the possibility that they may be dorsal ribs cannot be confidently excluded.

Pectoral girdle
The furcula is preserved in caudal view (Fig. 4C). It is 'Y'-shaped with straight furcular rami and an inclavicular angle of approximately 50°, similar to that of *Elsornis* and *Piscivorenantiornis*, but greater than that of *Shangyang* (Chiappe *et al*. 2007; M. Wang & Zhou 2017b, 2019). The hypocleidium is largely overlapped by the right scapula, but the exposed distal tip indicates that the hypocleidium has a length of approximately one-third that of the furcular rami, within the range of other bohaiornithids. The mediolateral compression of the hypocleidium present in the holotype and other bohaiornithids is visible at the base of this process, but not the distal tip due to poor preservation. The medial margins of the furcular rami project farther caudally than the lateral margins, rendering the caudal surface of the ramus concave, as in other enantiornithines (Chiappe & Walker 2002). The omal tips of the straight clavicular rami are expanded as in the holotype and other bohaiornithids (M. Wang *et al*. 2014). The articular surface for the coracoid is large and triangular, sloping caudoventrally and flat in the new specimen, while the slight depression in the holotype is most likely a preservational artefact.

The scapula is nearly as long as the femur, straight and ends in a blunt distal end as in the holotype and most other enantiornithines (Chiappe & Walker 2002; M. Wang & Liu 2016). Although the acromion processes are overlapped by the coracoids on both sides, the dorsal margin exposed on the right scapula indicates that it is dorsally directed relatively to the shaft, as in the holotype (M. Wang *et al*. 2014).

The right coracoid is preserved in dorsal view and is strut-like. The left one is ventrally exposed but mostly obscured by other elements. The acrocoracoid process is straight as in most enantiornithines (H. Hu & O'Connor 2017; O'Connor *et al*. 2017). The lateral margin is convex distally (Fig. 4B), being slightly less developed than

that observed in the holotype but still distinctly more convex than in other bohaiornithids (M. Wang *et al*. 2014; Fig. 4A). The sternal region of the coracoid body is coarse and porous, indicating incomplete ossification of the periosteal surface.

The sternum is completely preserved (Fig. 5A–C), compensating for anatomical features not accessible from the poorly preserved sternum in the holotype (Fig. 5D). The cranial margin is rounded as in the holotype, lacking the weakly developed craniolateral processes present in *Bohaiornis* and *Zhouornis* (Fig. 5E, F). The xiphoid process is well developed, as in most enantiornithines. Although in dorsal view, the keel is readily visible based on the convexity along the xiphoid process (which could also be confirmed in CL scanning), similar to *Bohaiornis* and *Gretcheniao* (D. Hu *et al*. 2011; Chiappe *et al*. 2019). The lateral trabeculae are broken in the holotype but are complete in IVPP V18693. They are caudolaterally oriented and extend to the level of the distal end of the xiphoid process. No distal expansion is present, differing from other bohaiornithids such as *Bohaiornis* (Fig. 5E; D. Hu *et al*. 2011), *Parabohaiornis* (M. Wang *et al*. 2014) and *Zhouornis* (Fig. 5F; Z. Zhang *et al*. 2013), which may be due to incomplete ossification. The intermediate trabeculae are weakly developed and considerably smaller than those of *Bohaiornis* and most other enantiornithines except for *Protopteryx* and the Pengornithidae, in which the intermediate trabeculae are absent, and *Eocathayornis* and *Longipteryx* (D. Hu *et al*. 2011; H. Hu *et al*. 2014; Li *et al*. 2014). A notch is present in the costal margin cranial to the base of the lateral trabecula, reminiscent of the condition in *Cathayornis* and *Longipteryx* (M. Wang & Liu 2016). The CL scans reveal that this notch is a genuine morphology rather an artefact of breakage (Fig. 5B). This notch is crushed in the holotype of *L. kurochkini* and *Parabohaiornis martini* (M. Wang *et al*. 2014) but is clearly observed in the holotypes of *Bohaiornis guoi* and *Zhouornis hani* (Fig. 5E, F), suggesting that this feature is a synapomorphy of bohaiornithids.

Forelimb
Most elements of the forelimbs are complete and remain in articulation except for some of the manual phalanges. The forelimb is slightly shorter than the hind limb (ratio of humerus + ulna + major metacarpal length/ femur + tibiotarsus + metatarsal III length = 0.95), similar to the condition in the holotype and *Bohaiornis*, whereas the forelimb exceeds the hind limb in length in *Parabohaiornis* as the result of a proportionally longer humerus (D. Hu *et al*. 2011; M. Wang *et al*. 2014).

The humerus is preserved in caudal view and is shorter than the ulna, as in the holotype. The shaft is
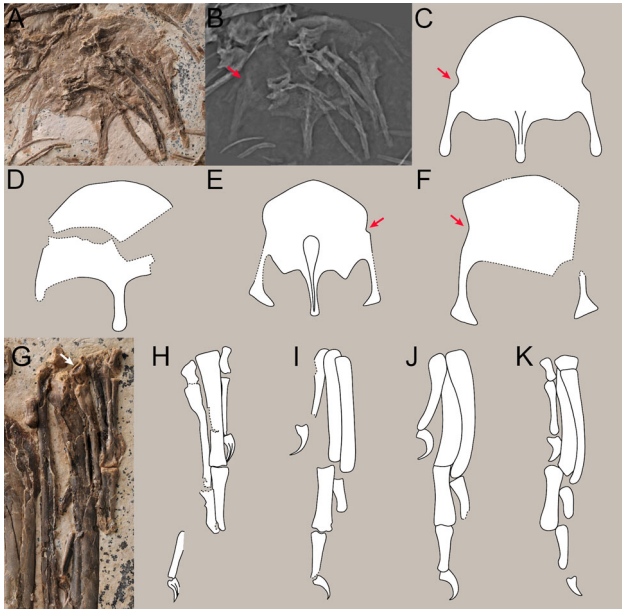
Figure 5. Comparison of sternums from selected bohaiornithids: **A,** photograph, **B,** CL image and **C,** reconstruction of *L. kurochkini* (IVPP V18693); **D,** *L. kurochkini* holotype (IVPP V17964); **E,** *Bohaiornis* (LPM B00167); and **F,** *Zhouornis* (BMNHC Ph756). D–F are modified from M. Wang *et al*. (2014), D. Hu *et al*. (2011) and Z. Zhang *et al*. (2013). Comparisons of hands in bohaiornithids: **G, H,** *L. kurochkini* (IVPP V18693, right); **I,** *L. kurochkini* holotype (IVPP V17964, left); **J,** *Zhouornis* (BMNHC Ph756, right); and **K,** *Bohaiornis* (LPM B00167). I–K modified from M. Wang *et al*. (2014), Y. Zhang *et al*. (2014) and D. Hu *et al*. (2011). Red arrows (B, C, E, F) indicate the concave area in the sternum lateral margin and the white arrow (G) indicates the concavity on the cranial surface of the minor metacarpal; the dashed lines indicate broken or overlapped margins.

sigmoidal with the proximal portion deflected ventrally and the distal end deflected dorsally, similar to the holotype and other bohaiornithids but less pronounced than in *Linyiornis* and *Pterygornis* (M. Wang *et al*. 2014, 2016; Y. Wang *et al*. 2016). Overall, the morphology of the humerus is consistent with that of the holotype. The ventral tubercle is separated from the humeral head by a shallow capital incision as in other enantiornithines. The ventrally projected proximal margin is concave in the central portion and convex dorsally and ventrally, also as in all enantiornithines (Chiappe & Walker 2002) with the exception of pengornithids. The dorsally projected deltopectoral crest is narrower than half the width of the humeral shaft and extends for approximately one-third of the length of the humerus. The distal end of the deltopectoral crest merges into the shaft gradually rather than ending abruptly as in some other enantiornithines, such as pengornithids (M. Wang *et al*. 2014; H. Hu *et al*. 2015).

The robust shaft of the ulna is bowed proximally and is straight distally, as in the holotype and most enantiornithines (Chiappe & Walker 2002; M. Wang *et al*. 2014). A weakly developed olecranon process is present, as in the holotype. The caudodorsal surface of the left radius preserves a groove similar to that in the holotype, but it is more weakly developed. The sub-rectangular semilunate carpal is unfused to the major metacarpal and is visible on the left.

The right hand is better preserved than the left, in which most phalanges are missing. The carpometacarpus is entirely unfused. The alular metacarpal is craniocaudally thinner than the proximal portion of both the major and the minor metacarpals. The alular metacarpal is approximately 30% the length of the major metacarpal. The major metacarpal is much more robust and nearly twice the width of the minor metacarpal, whereas this ratio appears slightly smaller in the holotype. Considering the flattened and partly overlapping preservation of the major and minor metacarpals in the holotype, this variance is most likely an artefact of preservation. The minor metacarpal is longer than the major metacarpal with the distal end extending further distally, which is typical of enantiornithines (Chiappe & Walker 2002). The proximal half of the left minor metacarpal is bowed, more obviously than in the holotype. The proximal portion of the right minor metacarpal is deflected by breakage and thus the cranial surface is exposed bearing a rounded concavity (Fig. 5G).

The alular digit is much thinner than the major digit and the alular ungual phalanx terminates level with the distal end of the major metacarpal (Fig. 5G, H). The proximal phalanx of the major digit is robust, being slightly wider than the major metacarpal itself, as observed in the holotype and other bohaiornithids (M. Wang *et al*. 2014). The right penultimate phalanx and ungual phalanx are preserved between the ulna and radius; the major digit ungual is subequal in size and curvature to that of the alular digit. Only one preserved phalanx forms the minor digit, as in other bohaiornithid specimens including the *L. kurochkini* holotype (Fig. 5I), *Bohaiornis guoi* (Fig. 5K; the holotype and referred specimen IVPP V17963), *Sulcavis geeorum* (holotype) and *Zhouornis hani* (Fig. 5J, the holotype and referred specimen BMNHC Ph 756) (D. Hu *et al*. 2011; O'Connor *et al*. 2013; Zhang *et al*. 2013; Li *et al*. 2014; M. Wang *et al*. 2014; Z. Y. Zhang *et al*. 2014). This may indicate that the ungual phalanx of the minor digit is fully reduced throughout the Bohaiornithidae.

Pelvic girdle
The pelvic girdle is well preserved in the new specimen. All elements are unfused. Both ilia are completely

preserved in lateral view, the left near the synsacrum (Fig. 4D) and the right near the left foot. The preacetabular wing is longer and dorsoventrally taller than the postacetabular wing, with a height ratio of approximately 2.3. Just cranial to the acetabulum, the preacetabular wing is dorsally expanded so that the dorsal margin is concave, whereas this margin is straight in many other enantiornithines, such as *Shangyang* and *Parapengornis* (H. Hu *et al*. 2015; M. Wang & Zhou 2019). The postacetabular ala tapers abruptly from the acetabulum forming a blunt caudal margin, similar to that in *Zhouornis* (Y. Zhang *et al*. 2014). The pubic pedicel is longer than the ischiadic pedicel as in other enantiornithines.

The right ischium and both pubes are preserved cranial to the pygostyle. The ischium is robust with a curved shaft, bearing a well-developed dorsal process similar to that of the holotype (M. Wang *et al*. 2014). Caudal to the dorsal process, a ridge-like structure is present in the lateral surface of the right ischium. The pubes are slender compared to the ischium. In both elements the shaft is curved so that the dorsal margin is concave, as observed in the holotype.

Hind limb
Both hind limbs are preserved although the left foot is partially disarticulated due to overlap with the ilium. The femur is nearly straight and measures 85% of the tibiotarsus in length, as in the holotype and most other enantiornithines (D. Hu *et al*. 2011; O'Connor *et al*. 2011; M. Wang *et al*. 2014; H. Hu & O'Connor 2017), but proportionately shorter than in pengornithids (H. Hu *et al*. 2015). The patellar groove is developed on the distal end.

The fibular crest is visible on the left tibiotarsus and exposed in cranial view; it measures approximately 30% the length of the tibiotarsus (Fig. 4H) as in *Bohaiornis*, *Monoenantiornis* and *Rapaxavis* (D. Hu *et al*. 2011; O'Connor *et al*. 2011; H. Hu & O'Connor 2017). Cnemial crests are absent as in the holotype and most other enantiornithines (M. Wang *et al*. 2014). The proximal tarsals are fused to each other and almost completely fused to the tibia, forming a true tibiotarsus. A large triangular ascending process can still be discerned on both sides (Fig. 4E, F). This is similar to the condition in the *Parabohaiornis martini* holotype and may be due to skeletal immaturity (H. Hu & O'Connor 2017). The fused distal proximal tarsals form the cranially projected distal condyles of the tibiotarsus. The ball-shaped medial condyle is transversely larger than the lateral condyle, as in the holotype, which is considered a primitive feature in basal birds (O'Connor *et al*. 2009). The better-preserved right fibula is expanded proximally and

sharply tapered distally, and is half the length of the tibiotarsus.

Metatarsal I is 'J'-shaped and short, measuring 28% of the length of metatarsal II, similar to the condition in most enantiornithines except for the pengornithids (H. Hu *et al*. 2015). Metatarsals III and IV are subequal in length and longer than metatarsal II. Metatarsal IV is considerably more slender than the other metatarsals, as in other enantiornithines (Chiappe & Walker 2002), and the distal end is deflected laterally from the long axis of the metatarsals (Fig. 4I).

The pedal digits are similar to those of other bohaiornithids in morphology with a short and reversed hallux. Digit II is remarkably more robust than all the other digits and the proximal phalanx is longer than the penultimate phalanx, similar to the holotype and other bohaiornithids (M. Wang *et al*. 2014). Digit IV is very delicate and measures only 70% of the length of digit III, with all of the phalanges subequal in length. Most of the ungual phalanges are well preserved in association with their respective keratinous sheaths. The ungual of digit I is slightly more robust and recurved compared to the others. The ungual of digit IV ungual is the shortest, and that of digit III is the longest and the least recurved, as in other bohaiornithids (Z. Zhang *et al*. 2013; Li *et al*. 2014; M. Wang *et al*. 2014; Y. Zhang *et al*. 2014). All unguals have well-developed ligamental grooves on the lateral surfaces and lack flexor tubercles.

Discussion

Phylogenetic analysis
The strict consensus tree from the phylogenetic analysis (Fig. 6) largely confirms previous results published by M. Wang & Zhou (2019) with regards to the placements of most clades, but with slightly better resolution inside both Enantiornithes and Ornithuromorpha. Hongshanornithidae is resolved as monophyletic within Ornithuromorpha, slightly differing from the position in the results of M. Wang & Zhou (2019), in that it is now basal to *Jianchangornis*. Pengornithidae and *Protopteryx* are resolved forming a clade in the basal-most position in the Enantiornithes, as in most previous analyses (M. Wang *et al*. 2016; H. Hu & O'Connor 2017; M. Wang & Zhou 2019). Longipterygidae is resolved as derived, as in M. Wang & Zhou (2019). The monophyly of Bohaiornithidae is also supported in this analysis and includes *Bohaiornis*, *Longusunguis*, *Parabohaiornis*, *Shenqiornis* and *Sulcavis*, although the position of *Zhouornis* outside of this clade differs from a previous analysis (M. Wang & Zhou 2019). IVPP V18693 is
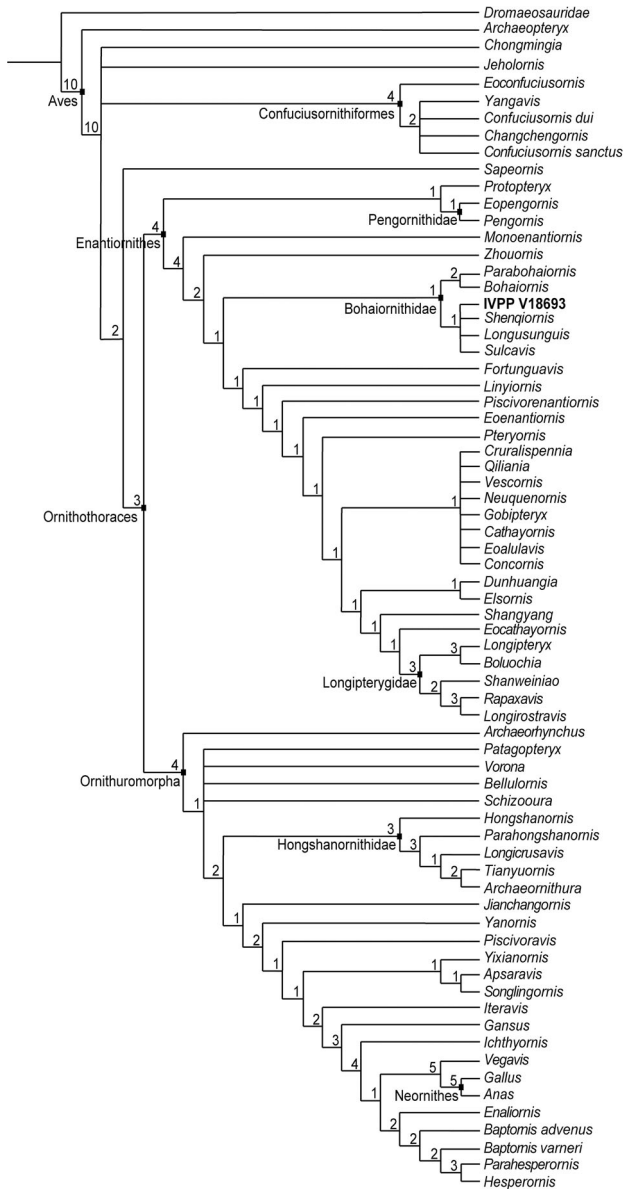
Figure 6. Strict consensus tree showing the phylogenetic position of IVPP V18693. Absolute calculated Bremer support values are indicated at each node.

resolved as a member of Bohaiornithidae and forms a polytomy with *Longusunguis*, *Shenqiornis* and *Sulcavis*, supporting the taxonomic inference based on morphological comparisons.

Postorbital bar

The new specimen of *L. kurochkini* (IVPP V18693) reveals important new morphological information regarding this taxon, as well as clarification of important transitions within Aves. The reduction and eventual loss

of the postorbital bar and appearance of the enlarged orbit and kinetic skull is one of the key modifications that occurs in the transition between non-avian dinosaurs and crown birds. Cranial kinesis is the movement of the rostrum relative to the braincase, allowing various advantages such as increased gape for swallowing large prey, more rapid opening/closing of the bill, increased bite force, greater precision in food selection, and specialized feeding strategies such as mud-probing and filtering (Zusi 1984; Estrella & Masero 2007; Gussekloo *et al.* 2017). All of these functions serve to improve feeding abilities and can be considered evolutionarily advantageous. The postorbital bar connects the braincase and the jugal tightly, excluding the possibility of rostrum movements relative to the braincase, thus its reduction and loss is one of the key contributions to the appearance of the flexible avian skull (Zusi 1984; Hou *et al.* 1999; Holliday & Witmer 2008; Bhullar *et al.* 2016).

Despite the importance of postorbital reduction in the evolution of cranial kinesis, little is known about the morphology and evolution of the postorbital in early birds, especially in stem ornithothoracines. All known non-ornithothoracine stem avians retain a plesiomorphically large postorbital and complete postorbital bar, as in *Archaeopteryx*, *Confuciusornis* and *Sapeornis* (Elzanowski *et al.* 2018; Rauhut *et al.* 2018; H. Hu *et al.* 2019; M. Wang *et al.* 2019). The postorbital of *Sapeornis* is broad and triangular in shape, with weaker concave margins than that of *Archaeopteryx*, similar to the condition in some dromaeosaurids such as *Linheraptor* (Fig. 7A; Xu *et al.* 2015; Rauhut *et al.* 2018; H. Hu *et al.* 2019). The more slender condition in *Archaeopteryx* resembles some non-avian theropods, such as the alvarezsaurid *Shuvuuia* (Chiappe *et al.* 1998). Despite the hundreds (perhaps thousands) of specimens referable to the Confuciusornithiformes, no published specimens clearly show the morphology of the postorbital, especially its boundaries with the braincase and the jugal, although the outline of the complete postorbital bar can be identified in several specimens (Chiappe *et al.* 1999; M. Wang *et al.* 2019).

Evidence regarding the postorbital is limited in the Enantiornithes and stem ornithuromorphs despite their high taxonomic diversity. Consequently, little can be said to regard whether, or to what degree, this element was reduced in the ornithothoracine common ancestor and in the members of these two lineages. In previously known enantiornithines the only unequivocal postorbitals are preserved in the indeterminate enantiornithine LP4450 and *Pengornis* (IVPP V15576) (Fig. 7A; Sanz *et al.* 1997; Zhou *et al.* 2008; O'Connor & Chiappe 2011). The frontal and squamosal processes of the
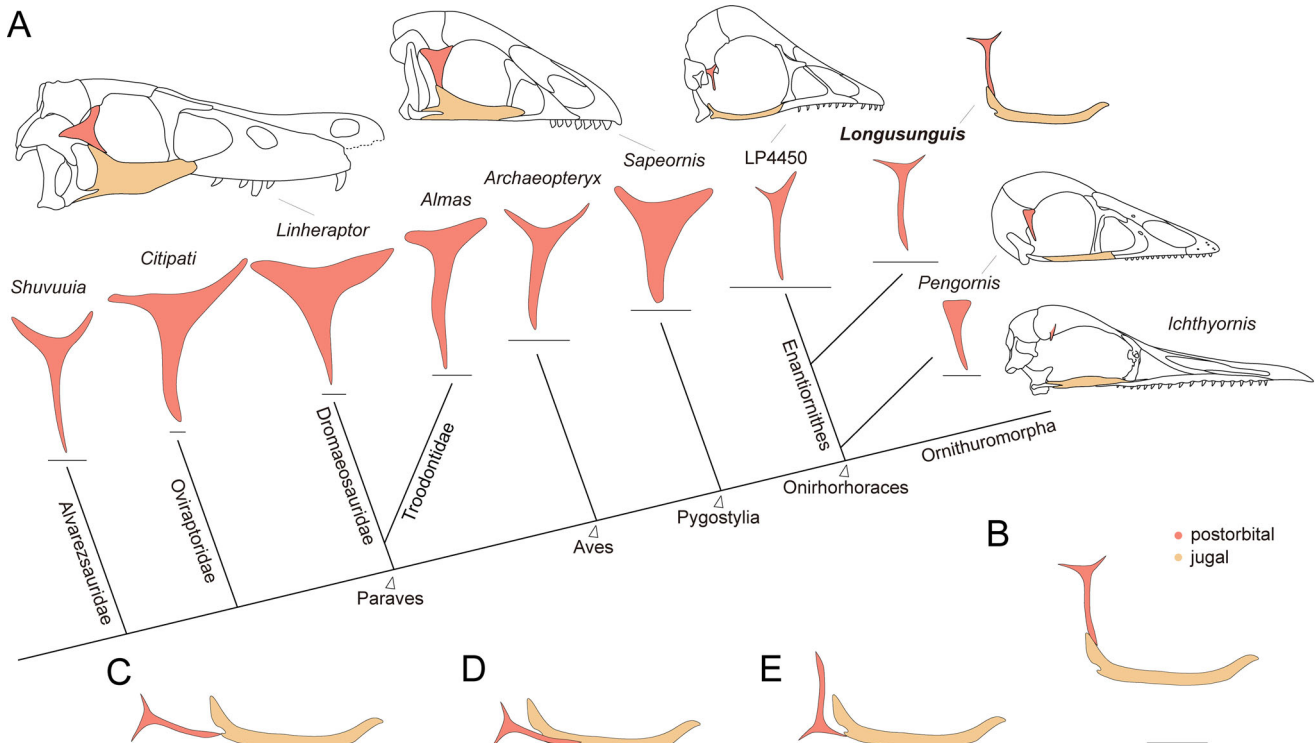
Figure 7. **A,** comparisons of postorbital bars in early birds and closely related non-avian dinosaurs (postorbitals: *Shuvuuia* follows Chiappe *et al*. [1998]; *Citipati* follows Clark *et al*. [2002]; *Linheraptor* follows Xu *et al*. [2015]; *Almas* follows Pei *et al*. [2017]; *Archaeopteryx* follows Rauhut *et al*. [2018]; *Sapeornis* modified from Pu *et al*. [2013] and D. Hu *et al*. [2010]; Enantiornithes LP4450 follows Sanz *et al*. [1997]; *Pengornis* follows O'Connor & Chiappe [2011]). Lateral line drawings of selected skulls: *Linheraptor* follows Xu *et al*. (2015) and M. Wang & Hu (2017); *Sapeornis* follows H. Hu *et al*. (2019); LP4450 follows M. Wang & Hu (2017); *Pengornis* modified from O'Connor & Chiappe (2011); *Ichthyornis* follows Field *et al*. (2018). Hypothetical reconstructions to determine if the triradiate element in *Longusunguis* (IVPP V18693) is a postorbital or a quadratojugal: **B,** reconstructed postorbital bar treating this element as a postorbital; **C–E,** reconstructed jugal bar alternatively treating this element as a quadratojugal, with its elongate process treated as a jugal process in C and D and squamosal process in E, where it turns out to be too long to be either the jugal or squamosal process of the quadratojugal. Scale bar = 5 mm.

postorbital are strongly reduced and only the jugal process is well developed in *Pengornis*, so that this element is semilunate in lateral view and has lost the contact with the jugal (Zhou *et al*. 2008). The postorbital in LP4450 retains the plesiomorphic triradiate morphology with a remarkably elongate jugal process, similar to but more slender than the condition in *Archaeopteryx* and differing from this basal-most taxon in that the jugal process does not reach the jugal, representing the break of a complete postorbital bar (Sanz *et al*. 1997). In the bohaiornithids *Shenqiornis* and *Sulcavis* disarticulated elements tentatively identified as the postorbital resemble the broad condition in *Sapeornis*, but without additional information we cannot confirm these interpretations due to their poor preservation (O'Connor & Chiappe 2011; O'Connor *et al*. 2013).

In IVPP V18693 two disarticulated elements near the jugals are identified as the postorbitals, displaying the typical triradiate shape of the paravian postorbital (Fig. 7A). The condition in *Longusunguis* differs from the

broad triangular postorbital of *Sapeornis*, but is remarkably similar to the slender and delicate morphology of this element in the stem avian *Archaeopteryx* (Rauhut *et al*. 2018) and some non-avian dinosaurs such as *Almas*, *Citipati*, *Dilong*, *Incisivosaurus* and *Juravenator* (Clark *et al*. 2002; Xu *et al*. 2002, 2004; Göhlich & Chiappe, 2006; Balanoff *et al*. 2009; Pei *et al*. 2017), as well as the enantiornithine LP4450. The articular surface for the squamosal also resembles that in the non-avian dinosaurs listed above (Fig. 3C).

Although disarticulated on both sides, the unique triradiate shape of this element rules out alternative identifications as any other cranial elements except for the quadratojugal. We explored treatment of this element as the quadratojugal and found out that it would be impossible for it to articulate with the jugal: if the elongate process is the jugal process, it would be too long to contact the jugal caudally (Fig. 7C), a groove on the lateral surface of the jugal to accommodate this process is absent, and the short processes would be unable to

articulate with the quadrate (Fig. 7D); the elongate process is also too long to be the squamosal process since no squamosal process of the quadratojugal in any known theropod, including birds, is longer than the jugal process (Fig. 7E). Therefore, we rule out the possibility that this element might represent a quadratojugal. Notably, based on our observations, disarticulated elements previously identified as the quadratojugal in other stem ornithothoracines such as *Archaeorhynchus*, *Pterygornis* and *Rapaxavis* (Zhou & Zhang 2006; O'Connor *et al*. 2011; M. Wang *et al*. 2016) should be re-examined in light of the possibility that they may actually be misidentified strongly reduced postorbitals.

Based on the remarkable length of the jugal process of the postorbital and the well-developed postorbital process of the jugal preserved in IVPP V18693, we conclude that these two processes contacted each other *in vivo*, forming a complete postorbital bar (Fig. 7B), similar to that in non-ornithothoracine birds. The presence of a complete postorbital bar in *Longusunguis* confirms that the plesiomorphic diapsid skull morphology was retained by at least some enantiornithines. Considering the loss of the postorbital–jugal contact, and consequent loss of the postorbital bar, in the indeterminate enantiornithine LP4450 and *Pengornis* (IVPP V15576), we suggest that the postorbital bar was probably lost multiple times independently within Enantiornithes. In *Longusunguis* (IVPP V18693) the squamosal is reduced such that the quadratojugal process is too short to contact the quadratojugal, indicating the absence of a closed quadrate foramen (Figs 3D, 7B). This suggests that during the evolution of the temporal area in at least one lineage of enantiornithines, the squamosal–quadratojugal contact was the first to be lost, followed by reduction of the infratemporal fenestra due to the loss of the postorbital–jugal contact. This may have occurred simultaneously with loss of the supratemporal fenestra as contact between the postorbital and squamosal was also lost due to the reduction of the postorbital, as observed in *Pengornis* (Zhou *et al*. 2008; O'Connor & Chiappe 2011).

Acknowledgements

Supplementary material

Supplementary material for this article can be accessed here: https://doi.org/10.1080/14772019.2020.1748133.

ORCID

Han Hu ⓘ http://orcid.org/0000-0001-5926-7306
Min Wang ⓘ http://orcid.org/0000-0001-8506-1213
Paul G. McDonald ⓘ http://orcid.org/0000-0002-9541-3304

References

Balanoff, A. M., **Xu, X.**, **Kobayashi, Y.**, **Matsufune, Y.** & **Norell, M. A.** 2009. Cranial osteology of the theropod dinosaur *Incisivosaurus gauthieri* (Theropoda: Oviraptorosauria). *American Museum Novitates*, **3651**, 1–35. doi:10.1206/644.1

Baumel, J. J. & **Witmer, L. M.** 1993. Osteologia. Pp. 45–132 in J. J. Baumel, K. S. King, J. E. Breazile, H. E. Evans & J. C. Vanden Berge (eds) *Handbook of avian anatomy: nomina anatomica avium*. 2nd edition. Nuttall Ornithological Club, Cambridge.

Bhullar, B. A. S., **Hanson, M.**, **Fabbri, M.**, **Pritchard, A.**, **Bever, G. S.** & **Hoffman, E.** 2016. How to make a bird skull: major transitions in the evolution of the avian cranium, paedomorphosis, and the beak as a surrogate hand. *Integrative and Comparative Biology*, **56**, 389–403. doi:10.1093/icb/icw069

Chiappe, L. M. 1995. The phylogenetic position of the Cretaceous birds of Argentina: Enantiornithes and *Patagopteryx deferrariisi*. *Frankfurt am Main: Courier Forschungsinstitut Senckenberg*, **181**, 55–63.

Chiappe, L. M. & **Walker, C. A.** 2002. Skeletal morphology and systematics of the Cretaceous Euenantiornithes (Ornithothoraces: Enantiornithes). Pp. 240–267 in L. M. Chiappe & L. M. Witmer (eds) *Mesozoic birds: above the heads of dinosaurs*. University of California Press, Berkeley.

Chiappe, L. M., **Norell, M. A.** & **Clark, J. M.** 1998. The skull of a relative of the stem-group bird *Mononykus*. *Nature*, **392**, 275–278. doi:10.1038/32642

Chiappe, L. M., **Lamb, J. P. Jr** & **Ericson, P. G. P.** 2002. New enantiornithine bird from the marine Upper Cretaceous of Alabama. *Journal of Vertebrate Paleontology*, **22**, 170–174.

Chiappe, L. M., **Ji, S.-A.**, **Ji, Q.** & **Norell, M. A.** 1999. Anatomy and systematics of the Confuciusornithidae (Theropoda: Aves) from the late Mesozoic of northeastern China. *Bulletin of the American Museum of Natural History*, **242**, 1–89.

Chiappe, L. M., **Suzuki, S.**, **Dyke, G. J.**, **Watabe, M.**, **Tsogtbaatar, K.** & **Barsbold, R.** 2007. A new enantiornithine bird from the Late Cretaceous of the Gobi desert. *Journal of Systematic Palaeontology*, **5**, 193–208. doi:10.1017/S1477201906001969

Chiappe, L. M., **Meng, Q. J. Serrano, F.**, **Sigurdsen, T.**, **Wang, M.**, **Bell, A.** & **Liu, D.** 2019. New *Bohaiornis*-like bird from the Early Cretaceous of China: enantiornithine interrelationships and flight performance. *PeerJ*, **7**, e7846. doi:10.7717/peerj.7846

Clark, J. M., **Norell, M. A.** & **Rowe, T.** 2002. Cranial anatomy of *Citipati osmolskae* (Theropoda, Oviraptorosauria), and a reinterpretation of the holotype of *Oviraptor philoceratops*. *American Museum Novitates*, **3364**, 1–24. doi:10.1206/0003-0082(2002)364<0001:CAOCOT>2.0.CO;2

Elzanowski, A. & **Wellnhofer, P.** 1996. Cranial morphology of *Archaeopteryx*: evidence from the seventh skeleton. *Journal of Vertebrate Paleontology*, **16**, 81–94. doi:10.1080/02724634.1996.10011286

Elzanowski, A., **Peters, D. S.** & **Mayr, G.** 2018. Cranial morphology of the Early Cretaceous bird *Confuciusornis*. *Journal of Vertebrate Paleontology*, **38**, e1439832. doi:10.1080/02724634.2018.1439832

Estrella, S. M. & **Masero, J. A.** 2007. The use of distal rhynchokinesis by birds feeding in water. *Journal of Experimental Biology*, **210**, 3757–3762. doi:10.1242/jeb.007690

Field, D. J., **Hanson, M.**, **Burnham. D.**, **Wilson, L. E.**, **Super, K.**, **Ehret, D.**, **Ebersole, J. A.** & **Bhullar, B. A.** 2018. Complete *Ichthyornis* skull illuminates mosaic assembly of the avian head. *Nature*, **557**, 96–100. doi:10.1038/s41586-018-0053-y

Göhlich, U. B. & **Chiappe, L. M.** 2006. A new carnivorous dinosaur from the Late Jurassic Solnhofen archipelago. *Nature*, **440**, 329–331. doi:10.1038/nature04579

Goloboff, P. A. & **Catalano, S. A.** 2016. TNT version 1.5, including a full implementation of phylogenetic morphometrics. *Cladistics*, **32**, 221–238. doi:10.1111/cla.12160

Gussekloo, S. W. S., **Berthaume, M. A.**, **Pulaski, D. R.**, **Westbroek, I.**, **Waarsing, J. H.**, **Heinen, R.**, **Grosse, I. R.** & **Dumont, E. R.** 2017. Functional and evolutionary consequences of cranial fenestration in birds. *Evolution*, **71**, 1327–1338. doi:10.1111/evo.13210

He, H., **Wang, X.**, **Zhou, Z.**, **Wang, F.**, **Boven, A.**, **Shi, G.** & **Zhu, R.** 2004. Timing of the Jiufotang Formation (Jehol Group) in Liaoning, northeastern China, and its implications. *Geophysical Research Letters*, **31**, L12605. doi:10.1029/2004GL019790

He, H., **Wang, X.**, **Jin, F.**, **Zhou, Z.**, **Wang, F.**, **Yang, L.**, **Ding, X.**, **Boven, A.** & **Zhu, R.** 2006. The 40 Ar/39 Ar dating of the early Jehol Biota from Fengning, Hebei Province, northern China. *Geochemistry, Geophysics, Geosystems*, **7**, Q04001. doi:10.1029/2005GC001083

Holliday, C. M. & **Witmer, L. M.** 2008. Cranial kinesis in dinosaurs: intracranial joints, protractor muscles, and their significance for cranial evolution and function in diapsids. *Journal of Vertebrate Paleontology*, **28**, 1073–1088. doi:10.1671/0272-4634-28.4.1073

Hou, L.-H., **Martin, L. D.**, **Zhou, Z.-H.**, **Feduccia, A.** & **Zhang, F.-C.** 1999. A diapsid skull in a new species of the primitive bird *Confuciusornis*. *Nature*, **399**, 679–682. doi:10.1038/21411

Hu, D., **Li, L.**, **Hou, L.** & **Xu, X.** 2010. A new sapeornithid bird from China and its implication for early avian evolution. *Acta Geologica Sinica*, **84**, 472–482. doi:10.1111/j.1755-6724.2010.00188.x

Hu, D., **Li, L.**, **Hou, L.-H.** & **Xu, X.** 2011. A new enantiornithine bird from the Lower Cretaceous of western Liaoning, China. *Journal of Vertebrate Paleontology*, **31**, 154–161. doi:10.1080/02724634.2011.546305

Hu, H. & **O'Connor, J. K.** 2017. First species of Enantiornithes from Sihedang elucidates skeletal development in Early Cretaceous enantiornithines. *Journal of Systematic Palaeontology*, **15**, 909–926. doi:10.1080/14772019.2016.1246111

Hu, H., **Zhou, Z.-H.** & **O'Connor, J. K.** 2014. A subadult specimen of *Pengornis* and character evolution in Enantiornithes. *Vertebrata PalAsiatica*, **52**, 77–97.

Hu, H., **O'Connor, J. K.** & **Zhou, Z.-H.** 2015. A new species of Pengornithidae (Aves: Enantiornithes) from the Lower Cretaceous of China suggests a specialized scansorial habitat previously unknown in early birds. *PLoS ONE*, **10**, e0126791. doi:10.1371/journal.pone.0126791

Hu, H., **Sansalone, G.**, **Wroe, S.**, **McDonald, P. G.**, **O'Connor, J. K.**, **Li, Z. H.**, **Xu, X.** & **Zhou, Z.-H.** 2019. Evolution of the vomer and its implications for cranial kinesis in Paraves. *Proceedings of the National Academy of Sciences of the United States of America*, **116**, 19571–19578. doi:10.1073/pnas.1907754116

Linnaeus, C. 1758. *Systema Naturae*. 10th edition. Salvii Laurentii Holmiae, Stockholm.

Li, Z.-H., **Zhou, Z.-H.**, **Wang, M.** & **Clarke, J. A.** 2014. A new specimen of large-bodied basal enantiornithine *Bohaiornis* from the Early Cretaceous of China and the inference of feeding ecology in Mesozoic birds. *Journal of Paleontology*, **88**, 99–108. doi:10.1666/13-052

O'Connor, J. K. 2009. *A systematic review of Enantiornithes (Aves: Ornithothoraces)*. Unpublished PhD thesis, University of Southern California, 600 pp.

O'Connor, J. K. 2019. The trophic habits of early birds. *Palaeogeography, Palaeoclimatology, Palaeoecology*, **513**, 178–195.

O'Connor, J. K. & **Chiappe, L. M.** 2011. A revision of enantiornithine (Aves: Ornithothoraces) skull morphology. *Journal of Systematic Palaeontology*, **9**, 135–157. doi:10.1080/14772019.2010.526639

O'Connor, J. K., **Chiappe, L. M.**, **Gao, C.** & **Zhao, B.** 2011. Anatomy of the Early Cretaceous enantiornithine bird *Rapaxavis pani*. *Acta Palaeontologica Polonica*, **56**, 463–475. doi:10.4202/app.2010.0047

O'Connor, J. K., **Zheng, X.-T.**, **Hu, H.**, **Wang, X.-L.** & **Zhou, Z.-H.** 2017. The morphology of *Chiappeavis magnapremaxillo* (Pengornithidae: Enantiornithes) and a comparison of aerodynamic function in Early Cretaceous avian tail fans. *Vertebrata PalAsiatica*, **55**, 1–18.

O'Connor, J. K., **Zhang, Y.**, **Chiappe, L. M.**, **Meng, Q.**, **Li, Q. G.** & **Liu, D.** 2013. A new enantiornithine from the Yixian Formation with the first recognized avian enamel specialization. *Journal of Vertebrate Paleontology*, **33**, 1–12. doi:10.1080/02724634.2012.719176

O'Connor, J. K., **Wang, X.**, **Chiappe, L. M.**, **Gao, C.**, **Meng, Q.**, **Cheng, X.** & **Liu, J.** 2009. Phylogenetic support for a specialized clade of Cretaceous enantiornithine birds with information from a new species. *Journal of Vertebrate Paleontology*, **29**, 188–204. doi:10.1080/02724634.2009.10010371

Pei, R., Norell, M. A., Barta, D. E., Bever, G. S., Pittman, M. & Xu, X. 2017. Osteology of a new Late Cretaceous troodontid specimen from Ukhaa Tolgod, Ömnögovi Aimag, Mongolia. *American Museum Novitates*, **3889**, 1–48. doi:10.1206/3889.1

Pu, H., Chang, H., Lü, J., Wu, Y., Xu, L., Zhang, J. & Jia, S. 2013. A new juvenile specimen of *Sapeornis* (Pygostylia: Aves) from the Lower Cretaceous of northeast China and allometric scaling of this basal bird. *Paleontological Research*, **17**, 27–39.

Rauhut, O. W. M., Foth, C. & Tischlinger, H. 2018. The oldest *Archaeopteryx* (Theropoda: Avialiae): a new specimen from the Kimmeridgian/Tithonian boundary of Schamhaupten, Bavaria. *PeerJ*, **6**, e4191. doi:10.7717/peerj.4191

Sanz, J. L., Chiappe, L. M., Pérez-Moreno, B. P., Moratalla, J. J., Hernández-Carrasquilla, F., Buscalioni, A. D., Ortega, F., Poyato-Ariza, F. J., Rasskin-Gutman, D. & Martinez-Delclòs, X. 1997. A nestling bird from the Lower Cretaceous of Spain: implications for avian skull and neck evolution. *Science*, **276**, 154–1546. doi:10.1126/science.276.5318.1543

Swisher, C., Wang, X., Zhou, Z., Wang, Y., Jin, F., Zhang, J., Xu, X., Zhang, F. & Wang, Y. 2002. Further support for a Cretaceous age for the feathered–dinosaur beds of Liaoning, China: new 40 Ar/39 Ar dating of the Yixian and Tuchengzi formations. *Chinese Science Bulletin*, **47**, 135–138.

Walker, C. A. 1981. New subclass of birds from the Cretaceous of South America. *Nature*, **292**, 51–53. doi:10.1038/292051a0

Wang, M. & Liu, D. 2016. Taxonomical reappraisal of Cathayornithidae (Aves: Enantiornithes). *Journal of Systematic Palaeontology*, **14**, 29–47. doi:10.1080/14772019.2014.994087

Wang, M. & Hu, H. 2017. A comparative morphological study of the jugal and quadratojugal in early birds and their dinosaurian relatives. *The Anatomical Record*, **300**, 62–75. doi:10.1002/ar.23446

Wang, M. & Zhou, Z. 2017a. The evolution of birds with implications from new fossil evidences. Pp. 1–26 in N. J. Maina (ed.) *The biology of the avian respiratory system*. Springer International Publishing, Switzerland.

Wang, M. & Zhou, Z. 2017b. A morphological study of the first known piscivorous enantiornithine bird from the Early Cretaceous of China. *Journal of Vertebrate Paleontology*, **37**, e1278702. doi:10.1080/02724634.2017.1278702

Wang, M. & Zhou, Z. 2019. A new enantiornithine (Aves: Ornithothoraces) with completely fused premaxillae from the Early Cretaceous of China. *Journal of Systematic Palaeontology*, **17**, 1299–1312. doi:10.1080/14772019.2018.1527403

Wang, M., Zhou, Z. & O'Connor, J. K. 2014. A new diverse enantiornithine family (Bohaiornithidae fam. nov.) from the Lower Cretaceous of China with information from two new species. *Vertebrata PalAsiatica*, **52**, 31–76.

Wang, M., Hu, H. & Li, Z. 2016. A new small enantiornithine bird from the Jehol Biota, with implications for early evolution of avian skull morphology. *Journal of Systematic Palaeontology*, **14**, 481–497. doi:10.1080/14772019.2015.1073801

Wang, M., O'Connor, J. K. & Zhou, Z. 2019. A taxonomical revision of the Confuciusornithiformes (Aves: Pygostylia). *Vertebrata PalAsiatica*, **57**, 1–37. doi:10.19615/j.cnki.1000-3118.180530

Wang, X., O'Connor, J. K., Zhao, B., Chiappe, L. M., Gao, C. & Cheng, X. 2010. New species of Enantiornithes (Aves: Ornithothoraces) from the Qiaotou Formation in northern Hebei, China. *Acta Geologica Sinica*, **84**, 247–256. doi:10.1111/j.1755-6724.2010.00156.x

Wang, Y., Wang, M., O'Connor, J. K., Wang, X., Zheng, X. & Zhang, X. 2016. A new Jehol enantiornithine bird with three-dimensional preservation and ovarian follicles. *Journal of Vertebrate Paleontology*, **36**, e1054496. doi:10.1080/02724634.2015.1054496

Xu, X., Cheng, Y.-N., Wang, X.-L. & Chang, C.-H. 2002. An unusual oviraptorosaurian dinosaur from China. *Nature*, **419**, 291–293. doi:10.1038/nature00966

Xu, X., Norell, M. A., Kuang, X., Wang, X., Zhao, Q. & Jia, C. 2004. Basal tyrannosauroids from China and evidence for protofeathers in tyrannosauroids. *Nature*, **431**, 680–684. doi:10.1038/nature02855

Xu, X., Pittman, M., Sullivan, C., Choiniere, J., Tan, Q., Clark, J., Norell, A. & Wang, S. 2015. The taxonomic status of the Late Cretaceous dromaeosaurid *Linheraptor exquisitus* and its implications for dromaeosaurid systematics. *Vertebrata PalAsiatica*, **53**, 29–62. doi:10.11646/zootaxa.2403.1.1

Zhang, F., Zhou, Z., Hou, L. & Gu, G. 2001. Early diversification of birds: evidence from a new opposite bird. *Chinese Science Bulletin*, **46**, 945–949. doi:10.1007/BF02900473

Zhang, Y., O'Connor, J. K., Liu, D., Meng, Q., Sigurdsen, T. & Chiappe, L. M. 2014. New information on the anatomy of the Chinese Early Cretaceous Bohaiornithidae (Aves: Enantiornithes) from a subadult specimen of *Zhouornis hani*. *PeerJ*, **2**, e407. doi:10.7717/peerj.407

Zhang, Z., Chiappe, L. M., Han, G. & Chinsamy, A. 2013. A large bird from the Early Cretaceous of China: new information on the skull of enantiornithines. *Journal of Vertebrate Paleontology*, **33**, 1176–1189. doi:10.1080/02724634.2013.762708

Zhou, Z. 2014. The Jehol Biota, an Early Cretaceous terrestrial Lagerstätte: new discoveries and implications. *National Science Review*, **1**, 543–559. doi:10.1093/nsr/nwu055

Zhou, Z. & Zhang, F. 2006. A beaked basal ornithurine bird (Aves, Ornithurae) from the Lower Cretaceous of China. *Zoologica Scripta*, **35**, 363–373. doi:10.1111/j.1463-6409.2006.00234.x

Zhou, Z., Clarke, J. & Zhang, F. 2008. Insight into diversity, body size and morphological evolution from the largest Early Cretaceous enantiornithine bird. *Journal of Anatomy*, **212**, 565–577. doi:10.1111/j.1469-7580.2008.00880.x

Zusi, R. L. 1984. A functional and evolutionary analysis of rhynchokinesis in birds. *Smithsonian Contributions to Zoology*, **395**, 1–40.